Multidirectional Functionally Graded Plates Exposed to Transient-Type Pressure Pulses

Terry Hause[a], Ph.D.

[a]Research Mechanical Engineer, U.S. Army RDECOM-TARDEC, Warren, MI 48397

ABSTRACT

Multidirectional functionally graded simply supported plates where the grading occurs symmetrically in all three coordinate directions exposed to time-dependent pressure pulses is considered. Within this context, the classical thin plate theory is adopted (CPT). The grading occurs in all three coordinate directions and is based on 3 independent polynomial and power law distributions. The equations of motion are derived through the use of Hamilton's Principle. By leveraging both approximate analytical and numerical techniques such as the Guassian-Quadrature method, The Galerkin-Method, and the 4th Order Runge-Kutta method, the dynamic response for various kinds of pressure pulses is presented. In a detailed fashion, the influence of the volume fraction indexes, various geometrical and material parameters, and the damping on the dynamic response is presented and analyzed. Finally validations are made with specialized cases found within the literature.

Key Words: Functionally Graded; Dynamic Response; Transient Response; Multi-directional; Plates; Pressure Pulses

Report Documentation Page

Form Approved
OMB No. 0704-0188

1. REPORT DATE	2. REPORT TYPE	3. DATES COVERED
17 DEC 2013	**Journal Article**	**06-05-2013 to 16-11-2013**

4. TITLE AND SUBTITLE
Multidirectional Functionally Graded Plates Exposed to Transient-Type Pressure Pulses

5a. CONTRACT NUMBER

5b. GRANT NUMBER

5c. PROGRAM ELEMENT NUMBER

6. AUTHOR(S)
Terry Hause

5d. PROJECT NUMBER

5e. TASK NUMBER

5f. WORK UNIT NUMBER

7. PERFORMING ORGANIZATION NAME(S) AND ADDRESS(ES)
U.S. Army TARDEC,6501 East Eleven Mile Rd,Warren,Mi,48397-5000

8. PERFORMING ORGANIZATION REPORT NUMBER
#24372

9. SPONSORING/MONITORING AGENCY NAME(S) AND ADDRESS(ES)
U.S. Army TARDEC, 6501 East Eleven Mile Rd, Warren, Mi, 48397-5000

10. SPONSOR/MONITOR'S ACRONYM(S)
TARDEC

11. SPONSOR/MONITOR'S REPORT NUMBER(S)
#24372

12. DISTRIBUTION/AVAILABILITY STATEMENT
Approved for public release; distribution unlimited

13. SUPPLEMENTARY NOTES

14. ABSTRACT
Multidirectional functionally graded simply supported plates where the grading occurs symmetrically in all three coordinate directions exposed to time-dependent pressure pulses is considered. Within this context, the classical thin plate theory is adopted (CPT). The grading occurs in all three coordinate directions and is based on 3 independent polynomial and power law distributions. The equations of motion are derived through the use of Hamilton?s Principle. By leveraging both approximate analytical and numerical techniques such as the Guassian-Quadrature method, The Galerkin-Method, and the 4th Order Runge-Kutta method, the dynamic response for various kinds of pressure pulses is presented. In a detailed fashion, the influence of the volume fraction indexes, various geometrical and material parameters, and the damping on the dynamic response is presented and analyzed. Finally validations are made with specialized cases found within the literature.

15. SUBJECT TERMS
Functionally Graded; Dynamic Response; Transient Response; Multi-directional; Plates; Pressure Pulses

16. SECURITY CLASSIFICATION OF:			17. LIMITATION OF ABSTRACT	18. NUMBER OF PAGES	19a. NAME OF RESPONSIBLE PERSON
a. REPORT	b. ABSTRACT	c. THIS PAGE			
unclassified	**unclassified**	**unclassified**	**Public Release**	**36**	

1. Introduction

Plate and shell-type structural elements find themselves in all kinds of structures such as buildings, automobiles, and aircraft/spacecraft. Their structural design should be based on considerations such as temperature, material composition, geometrical attributes, and the types of loadings that they will be exposed to, whether static or dynamic. There is an exhaustive literature base devoted to the structural response of isotropic, laminated composites, unidirectional and bi-directional functionally graded plates and shells under various kinds of loadings based on the classical plate theories to the most advanced plate and shell theories. Although there remain gaps that need to be filled within the present literature base, a new frontier that yet remains to be explored and developed is the idea of multi-directional functionally graded plates where the material properties vary in all three coordinate directions as opposed to unidirectional or bidirectional orientations. This brings to the forefront the idea of spatial tailoring; whereby the distribution of the constituent materials in all three coordinate directions can be manipulated to achieve an optimal material distribution to achieve an optimum structural design to maintain its structural integrity within its operating environment. This concept is analogous to structural tailoring for laminated unidirectional composites whereby the ply-angle is manipulated to achieve an optimum configuration.

Based on a comprehensive literature review, a theoretical base which to build upon is found to be nonexistent. A brief synopsis on how to approach and theoretically model multidirectional functionally graded plates incorporating thermal effects, with the idea of spatial tailoring, has been introduced by [2] and [3]. With this in mind, a basic theoretical foundation of the

multidirectional functionally graded plates based on a linear classical thin plate theory under various types of dynamic loadings for the case of simply supported plates is developed. Within this theoretical foundation are the inclusion of damping effects and the transverse inertia.

2. Basic Assumptions and Preliminaries

Shown, in Fig. 1, is a pictorial representation of a multidirectional functionally graded plate referred to an Orthogonal Cartesian Coordinate System (x, y, z), where z is measured positive in the upwards direction from the mid-surface of the plate. While, *h* is the uniform thickness of the plate. Let any two constituent materials comprise a functionally graded plate. Then a generic property $P(x, y, z)$ can be expressed in terms of the volume fraction as

$$P(x, y, z) = [P_1 - P_2]V_1(x, y, z) + P_2 . \tag{1}$$

Where,

$$V_1(x, y, z) = V_{cx}(x)V_{cy}(y)V_{cz}(z) . \tag{2}$$

The chosen functional relationships for the volume fractions, $V_{cx}(x)$, $V_{cy}(y)$, and $V_{cz}(z)$ are given in a polynomial and power form as

$$V_{cx}(x) = \left[\frac{x}{L_1}\left(1 - \frac{x}{L_1}\right)\right]^{N_1}, \tag{3a}$$

$$V_{cy}(y) = \left[\frac{y}{L_2}\left(1 - \frac{y}{L_2}\right)\right]^{N_2}, \tag{3b}$$

$$V_{cz}(z) = \left(\frac{z}{h/2}\right)^{M}\left(\frac{1+\text{sgn}(z)}{2}\right) + \left(\frac{-z}{h/2}\right)^{M}\left(\frac{1-\text{sgn}(z)}{2}\right) \tag{3c}$$

The Signum function is defined as

$$\text{sgn}(z) = \begin{cases} 1, & z > 0 \\ 0, & z = 0 \\ -1 & z < 0 \end{cases} \tag{4}$$

N_1, N_2, and M are referred to as the volume fraction indexes providing a measure of the variation of the material profile through the structure in all three coordinate directions. It should be noted that this chosen grading of the constituent materials throughout the plate expresses a symmetric distribution in all three coordinate directions. Also, depending on the 3D grading desired, other possible functional relationships for the volume fraction are possible such as in the anti-symmetric case.

A detailed graphical depiction of each of the three directional volume fractions given as function of the volume fraction index and their respective coordinate direction is provided in Fig. (2)-(4) below. Looking at Fig. (2), which displays the volume fraction as a function of the distance along the plate in the *x*-direction for various magnitudes of the volume fraction indexes N_1, it is apparent that as $N_1 \to 0$, the volume fraction measure, $V_{cx}(x) \to 1$. As $N_1 \to \infty$ or becomes much larger than zero, $V_{cx}(x) \to 0$; While other volume fraction indexes produce volume fractions falling between these two extremes. The same exact behavior is seen in Fig. (3) where the volume fraction is presented as a function of the distance along the plate in the *y*-coordinate direction for various volume fraction indexes, N_2. In Fig. (4), The volume fraction as

a function of the through-the-thickness coordinate in the z-coordinate direction for various volume fraction indexes is depicted. When *M*=0, the volume fraction, $V_{cz}(z) = 1$; While $V_{cz}(z) = 0$ as $M \to \infty$ or becomes very large. All other volume fraction index values for *M*, give volume fractions in between the two extremes.

With this information in hand, Table 1. below, gives a summary for the possible types of functional grading, depending on the measure of the volume fraction index.

The chosen constituent materials for this paper are ceramic and metal. This leads to the expression of the material properties given by

$$[E(x, y, z),\ \rho(x, y, z)] = [E_{cm}\ ,\ \rho_{cm}\ ]V_1(x, y, z) + [E_m\ ,\ \rho_m\ ] \tag{5}$$

Where,

$$E_{cm} = E_c - E_m\ , \qquad \rho_{cm} = \rho_c - \rho_m\ . \tag{6}$$

The variation of Poisson's ratio, $\nu(x, y, z)$, is approximated as being constant throughout the material grading of the structure.

3. The strain-Displacement Relationships

For the classical plate theory, the strain-displacement relationships are provided as [6] (7)

$$e_{xx} = \frac{\partial u_0}{\partial x} - z\frac{\partial^2 w_0}{\partial x^2} \tag{8a}$$

$$e_{yy} = \frac{\partial \upsilon_0}{\partial y} - z\frac{\partial^2 w_0}{\partial y^2} \tag{8b}$$

$$\gamma_{xy} = \frac{\partial u_0}{\partial y} + \frac{\partial \upsilon_0}{\partial x} - 2z\frac{\partial^2 w_0}{\partial x \partial y} \tag{8c}$$

$$\gamma_{xz} = \gamma_{yz} = e_{zz} = 0 \tag{8d}$$

Where, (u_0, v_0, w_0) are 2-D displacement quantities of the mid-surface of the plate.

4. Constitutive Equations

The constitutive equations for a point-wise isotropic material for plane stress are given by

$$\begin{Bmatrix} \sigma_{xx} \\ \sigma_{yy} \\ \tau_{xz} \end{Bmatrix} = \begin{bmatrix} Q_{11}(x,y,z) & Q_{12}(x,y,z) & 0 \\ Q_{12}(x,y,z) & Q_{22}(x,y,z) & 0 \\ 0 & 0 & Q_{66}(x,y,z) \end{bmatrix} \begin{Bmatrix} e_{xx} \\ e_{yy} \\ 2e_{xy} \end{Bmatrix} \tag{9}$$

Where the material stiffnesses, $Q_{ij}(x,y,z)$, (i, j=1,2,6) are given by

$$Q_{11} = Q_{22} = \frac{E(x,y,z)}{1-\nu^2}, \quad Q_{12} = \frac{\nu E(x,y,z)}{1-\nu^2}, \quad Q_{66} = \frac{E(x,y,z)}{2(1+\nu)} \tag{10}$$

5. Equations of Motion

Adopting an energy approach, the equations of motion are derived through the use of Hamilton's Principle which is expressed as

$$\delta J = \delta \int_{t_0}^{t_1} (T - U + V)\, dt = 0 \tag{11}$$

Where t_0, t_1 are two arbitrary instants in time. *U* denotes the strain energy, *V* denotes the work, and *T* denotes the kinetic energy of the structure, while δ is the variational operator. Without

explicitly providing the individual energy terms they are assumed into the energy functional where the energy functional is expressed as

$$\int_{t_0}^{t_1}\Bigg[-\int_{\Omega}\int_{-\frac{h}{2}}^{\frac{h}{2}}(\sigma_{xx}\delta e_{xx}+\sigma_{yy}\delta e_{yy}+\tau_{xy}\gamma_{xy})dzd\,\Omega+\int_{\Omega}\rho(x,y)\ddot{w}_0\delta w_0\,d\Omega + \int_{\Omega}[P_t(x,y,t)-\mu(x,y)\dot{w}_0)]\delta w_0\,d\Omega\Bigg]dt=0 \tag{12}$$

Ω denotes the mid-surface area of the plate, P_t is the distributed force at the top surface, and $\mu(x,y)$ is the damping coefficient per unit area of the plate.

Considering Eqs. (8a-d), (9), and (12), and carrying out the integration throughout the thickness, integrating by parts where ever feasible, and taking into consideration the arbitrary and independent character of variations results in three equations of motion along with the associated boundary conditions in terms of displacements. The equations of motion are determined as

$$A_{11}(x,y)\frac{\partial^2 u_0}{\partial x^2}+[A_{12}(x,y)+A_{66}(x,y)]\frac{\partial^2 \upsilon_0}{\partial x\partial y}+A_{66}(x,y)\frac{\partial^2 u_0}{\partial x^2}+\frac{\partial A_{11}(x,y)}{\partial x}\frac{\partial u_0}{\partial x}+ \frac{\partial A_{66}(x,y)}{\partial y}\left(\frac{\partial u_0}{\partial y}+\frac{\partial \upsilon_0}{\partial x}\right)+\frac{\partial A_{12}(x,y)}{\partial x}\frac{\partial \upsilon_0}{\partial y}=0 \tag{13}$$

$$A_{22}(x,y)\frac{\partial^2 \upsilon_0}{\partial y^2}+[A_{12}(x,y)+A_{66}(x,y)]\frac{\partial^2 u_0}{\partial x\partial y}+A_{66}(x,y)\frac{\partial^2 \upsilon_0}{\partial x^2}+\frac{\partial A_{22}(x,y)}{\partial y}\frac{\partial \upsilon_0}{\partial y}+ \frac{\partial A_{66}(x,y)}{\partial x}\left(\frac{\partial u_0}{\partial y}+\frac{\partial \upsilon_0}{\partial x}\right)+\frac{\partial A_{12}(x,y)}{\partial y}\frac{\partial u_0}{\partial x}=0 \tag{14}$$

$$D_{11}(x,y)\nabla^4 w_0 + 2\frac{\partial D_{11}(x,y)}{\partial x}\frac{\partial(\nabla^2 w_0)}{\partial x} + 2\frac{\partial D_{11}(x,y)}{\partial y}\frac{\partial(\nabla^2 w_0)}{\partial y} + \nabla^2 D_{11}(x,y)(\nabla^2 w_0)$$
$$-(1-\nu)\left(\frac{\partial^2 D_{11}(x,y)}{\partial x^2}\frac{\partial^2 w_0}{\partial y^2} - 2\frac{\partial^2 D_{11}(x,y)}{\partial x\partial y}\frac{\partial^2 w_0}{\partial x\partial y} + \frac{\partial^2 D_{11}(x,y)}{\partial y^2}\frac{\partial^2 w_0}{\partial x^2}\right) + \rho(x,y)\ddot{w}_0 \qquad (15)$$
$$+ \mu(x,y)\dot{w}_0 = P_t(x,y,t)$$

As a result of the decoupling of the first two equations of motion which are in terms of the in-plane displacements, the third equation of motion in terms of the transverse displacements becomes the governing equation of motion. The reduced governing system of equations along with the associated boundary conditions becomes

$$\delta w_0 : \quad D_{11}(x,y)\nabla^4 w_0 + 2\frac{\partial D_{11}(x,y)}{\partial x}\frac{\partial(\nabla^2 w_0)}{\partial x} + 2\frac{\partial D_{11}(x,y)}{\partial y}\frac{\partial(\nabla^2 w_0)}{\partial y} + \qquad (16)$$
$$\nabla^2 D_{11}(x,y)(\nabla^2 w_0) - (1-\nu)\left(\frac{\partial^2 D_{11}(x,y)}{\partial x^2}\frac{\partial^2 w_0}{\partial y^2} - 2\frac{\partial^2 D_{11}(x,y)}{\partial x\partial y}\frac{\partial^2 w_0}{\partial x\partial y} + \right.$$
$$\left.\frac{\partial^2 D_{11}(x,y)}{\partial y^2}\frac{\partial^2 w_0}{\partial x^2}\right) + \rho(x,y)\ddot{w}_0 + \mu(x,y)\dot{w}_0 = P_t(x,y,t)\,.$$

For simply supported boundary conditions, the boundary constraints are expressed as

Along the edges $x = (0, L_1)$

$$w_0 = 0, \qquad -D_{11}(x,y)\frac{\partial^2 w_0}{\partial x^2} - D_{12}(x,y)\frac{\partial^2 w_0}{\partial y^2} = 0 \qquad (17)$$

Along the edges $x = (0, L_2)$

$$w_0 = 0, \qquad -D_{22}(x,y)\frac{\partial^2 w_0}{\partial y^2} - D_{12}(x,y)\frac{\partial^2 w_0}{\partial x^2} = 0\,. \tag{18}$$

The global stiffness quantities appearing within the equations of motion are defined as

$$[A_{ij}(x,y), B_{ij}(x,y), D_{ij}(x,y)] = \int_{-\frac{h}{2}}^{\frac{h}{2}} Q_{ij}(x,y,z)(1,z,z^2)dz\,, \qquad (i,\, j = 1,\, 2,\, 6) \tag{19}$$

For the case of symmetric grading in all three coordinate directions, $[B_{ij}] = 0$. With the use of Eqs. (5) and (10), and carrying out the indicated integration within Eq. (19), the global stiffness quantities can be expressed as

$$(A_{ij}, B_{ij}, D_{ij}) = \frac{1}{1-\nu^2}(E_1, E_2, E_3) \qquad (i, j=1,2,6) \tag{20a}$$

$$(A_{66}, B_{66}, D_{66}) = \frac{1}{2(1+\nu)}(E_1, E_2, E_3) \tag{20b}$$

Where,

$$E_1(x,y) = \frac{E_{cm}\,h}{M+1}V_{cx}(x)V_{cy}(y) + hE_m\,, \tag{21a}$$

$$E_2(x,y) = 0 \tag{21b}$$

$$E_3(x,y) = \frac{E_{cm}\,h^3}{4(M+3)}V_{cx}(x)V_{cy}(y) + \frac{E_m h^3}{12} \tag{21c}$$

6. Solution Methodology

As part of the solution process of Eq. (16), the Galerkin Method is leveraged which requires that both the essential (kinematic) and natural boundary conditions be fulfilled. To achieve this

requirement, the transverse displacement, $w_0(x, y)$ and the transverse pressure, $P_t(x, y, z)$ are both expressed in terms of a Navier-type expression given as

$$w(x, y, t) = W(t)\sin(\lambda_m x)\sin(\mu_n y) \tag{22}$$

Where $\lambda_m = m\pi/L_1$, $\mu_n = n\pi/L_2$ and (m ,n) are the number of sine half-waves in the corresponding directions; While,

$$P_t(x, y, t) = P_{mn}(t)\sin(\lambda_m x)\sin(\mu_n y) \tag{23}$$

Where,

$$P_{mn}(t) = \frac{4}{L_1 L_2}\int_0^{L_2}\int_0^{L_1} P_t(x, y, t)\sin(\lambda_m x)\sin(\mu_n y)\,dxdy \tag{24}$$

with $P_t(x, y, t) = P_t(t)$, and integrating gives

$$P_{mn}(t) = 16\,P_t(t)\big/mn\,\pi^2 \tag{25}$$

Where, $P_t(t)$ is the desired transverse pressure. With these expressions in hand and applying the Galerkin Method to Eqs (16), utilizing Eqs. (22), (23), and (25), gives

$$I_{mn}\ddot{W}_{mn}(t) + C_{mn}\dot{W}_{mn}(t) + K_{mn}W_{mn}(t) = \frac{16\,P_t(t)}{mn\,\pi^2}, \tag{26}$$

Where $W_{mn}(t)$ is the amplitude of deflection, I_{mn} is the plate inertia, C_{mn} is the overall damping coefficient of the plate, and K_{mn} is the overall stiffness of the plate all of which are given as

$$K_{mn} = \int_0^{L_2}\int_0^{L_1}\Big[\left(\lambda_m^2 + \mu_n^2\right)^2 D_{11}(x,y)s_{mx}^2 s_{ny}^2 - 2\lambda_m\left(\lambda_m^2 + \mu_n^2\right)^2 \frac{\partial D_{11}(x,y)}{\partial x} c_{mx}\, s_{mx}\, s_{ny}^2 - \tag{27}$$

$$- 2\mu_n\left(\lambda_m^2 + \mu_n^2\right)^2 \frac{\partial D_{11}(x,y)}{\partial y} s_{mx}^2 c_{ny}\, s_{ny} - \left(\lambda_m^2 + \nu\mu_n^2\right)\frac{\partial^2 D_{11}(x,y)}{\partial x^2} s_{mx}^2 s_{ny}^2 +$$

$$+ 2\lambda_m\mu_n(1-\nu)\frac{\partial^2 D_{11}(x,y)}{\partial x \partial y} c_{mx}\, s_{mx}\, c_{ny}\, s_{ny} - \left(\mu_n^2 + \nu\lambda_m^2\right)\frac{\partial^2 D_{11}(x,y)}{\partial y^2} s_{mx}^2 s_{ny}^2\Big] dxdy$$

$$C_{mn} = \int_0^{L_2}\int_0^{L_1} \mu(x,y) s_{mx}^2 s_{ny}^2\, dxdy \tag{28}$$

$$I_{mn} = \int_0^{L_2}\int_0^{L_1} \rho_0(x,y) s_{mx}^2 s_{ny}^2\, dxdy \tag{29}$$

Within the above expressions,

$$c_{mx} = \cos(m\pi x/L_1), \qquad s_{mx} = \sin(m\pi x/L_1) \tag{30a,b}$$

$$c_{ny} = \cos(n\pi y/L_2), \qquad s_{ny} = \sin(n\pi y/L_2) \tag{31a,b}$$

Normalizing Eq. (26) results in,

$$\ddot{W}_{mn}(t) + 2\Delta_{mn}\omega_{mn}\dot{W}_{mn}(t) + \omega_{mn}^2 W_{mn}(t) = \tilde{P}_{mn}(t) \tag{32}$$

where $\omega_{mn} = \sqrt{K_{mn}/I_{mn}}$ is the natural frequency of the plate, $\Delta_{mn} = C_{mn}/2I_{mn}\omega_{mn}$ is the overall normalized damping coefficient, and $\tilde{P}_{mn}(t) = 16\,P_t(t)/mn\,\pi^4 I_{mn}$ is the normalized transverse pressure.

7. **Transverse Pressure Loadings**

In a dynamic world, structures can experience many different types of external excitations from a variety of causes or sources. Whether constant or time-varying they are the driving force for their dynamic motion. In the supersonic and hypersonic world, aircraft can experience various types of pressure waves which can appear as violent/hostile disturbances which can materialize from a variety of environmental conditions. Sonic boom is one such example which occurs during the transition from subsonic speeds to supersonic speeds. Also, ground combat vehicles can experience various types of external excitations from explosives, gun fire, and electromagnetic pulses, etc. This generates the need to understand these types of excitations and their effect from a structural response standpoint for design purposes. Some of the more common transverse pressure pulses are presented below.

The sonic boom over pressure which commonly materializes from exceeding the speed of sound is expressed mathematically as [5]

$$P_t(t) = \begin{cases} P_0\left(1 - t/t_p\right) & \text{for} \quad 0 < t < rt_p \\ 0 & \text{for} \quad t < 0 \quad \textit{and} \quad t > rt_p \end{cases} \tag{33}$$

Where P_0 denotes the peak reflected pressure above ambient, t_p denotes the positive time duration, from the time of impact, and *r* denotes the shock pulse length factor. The expression for the sonic boom can be expressed functionally in contrast to a piecewise formulation as

$$P_t(t) = P_0\left(1 - t/t_p\right)\left[H(t) - H(t - rt_p)\right] \tag{34}$$

Where $H(t)$ denotes the Heaviside Step Function. This implies that the normalized pressure $\tilde{P}_{mn}(t)$ becomes

$$\tilde{P}_{mn}(t) = \frac{16 P_0}{mn \pi^2 I_{mn}} \left(1 - t/t_p\right)\left[H(t) - H(t - rt_p)\right] \tag{35}$$

As special cases of the sonic boom, when $r = 1$, the waveform degenerates into a triangular pulse. When $r = 2$, The sonic boom waveform becomes symmetric. When $r \neq 2$ a non-symmetric N-Pulse shape waveform is produced. Finally, when $r = 1$ and $t_p \to \infty$ a step pulse is realized. For the case of the step pulse, the normalized pressure $\tilde{P}_{mn}(t)$ is expressed as

$$\tilde{P}_{mn}(t) = \frac{16 P_0}{mn \pi^2 I_{mn}} \qquad \text{for} \quad t > 0 \tag{36}$$

As an additional case, a rectangular pulse can be formulated as

$$\tilde{P}_{mn}(t) = \frac{16 P_0}{mn \pi^2 I_{mn}} \left[H(t) - H(t - t_p)\right]. \tag{37}$$

Also under consideration, is a air blast wave traveling tangentially/parallel to the plate which is given as

$$P_t(t) = P_0 e^{-\eta(ct - x_1)} H(ct - x_1) \tag{38}$$

The normalized pressure $\tilde{P}_{mn}(t)$ then becomes

$$\tilde{P}_{mn}(t) = \frac{16 P_0}{mn \pi^2 I_{mn}} \left[e^{-\eta(ct - x_1)} H(ct - x_1)\right] \tag{39}$$

Where c is the wave speed within the surrounding medium which in this is air; while η is a blast decay parameter. Finally a sine pulse is considered which is expressed mathematically as

$$P_t(t) = \begin{cases} P_0 \sin(\pi t/t_p), & \text{for} \quad 0 \le t \le t_p \\ 0 & \text{for} \quad t > t_p \end{cases} \tag{40}$$

Functionally it is expressed as

$$P_t(t) = P_0 \sin(\pi\, t/t_p)\left[H(t) - H(t - t_p)\right] \tag{41}$$

Where the normalized pressure becomes

$$\tilde{P}_{mn}(t) = \frac{16\,P_0}{mn\,\pi^2 I_{mn}} \sin(\pi\, t/t_p)\left[H(t) - H(t - t_p)\right] \tag{42}$$

8. Results and Discussion

To validate the present theory, validations are made by simplifying the governing response equation (Eq. 26) for the case of an isotropic plate based on the linear classical plate theory (CPT) for thin plates. Both the deflection-time response and the natural frequency response are validated. The deflection-time response for the linear CPT is compared with Akay[1] who presents results for both the linear and nonlinear cases for a constant uniform loading. The natural frequencies for the first ten modes are compared against the exact values provided by Ramu and Mohanty [4] for the linear CPT.

8.1 Validation of the deflection-time response

As an aside, for the case of a uniform loading the transverse pressure is expressed as

$$P = P_0 \sin(\pi x/L_1) \sin(\pi y/L_2)\,. \tag{43}$$

In this case, Eq. (26) becomes,

$$I_{mn}\ddot{W}_{mn}(t) + C_{mn}\dot{W}_{mn}(t) + K_{mn}W_{mn}(t) = \frac{4P_0L_1L_2}{\pi^2}; \tag{44}$$

While for the case of a isotropic plate,

$$D_{11}(x,y) = D = \frac{Eh^3}{12(1-\nu^2)}, \tag{45}$$

$$\frac{\partial D_{11}(x,y)}{\partial x} = \frac{\partial D_{11}(x,y)}{\partial y} = \frac{\partial^2 D_{11}(x,y)}{\partial x^2} = \frac{\partial^2 D_{11}(x,y)}{\partial x \partial y} = \frac{\partial^2 D_{11}(x,y)}{\partial y^2} = 0 \tag{46}$$

$$K_{mn} = \frac{D\left(\lambda_m^2 + \mu_n^2\right)^2 L_1 L_2}{4},\ I_{mn} = \frac{\rho h L_1 L_2}{4},\ C_{mn} = 0 \text{ (No damping assumed).} \tag{47a-c}$$

Dividing through by I_{mn} gives

$$\ddot{W}_{mn}(t) + \omega_{mn}^2 W_{mn}(t) = \tilde{P}, \tag{48}$$

Where $\omega_{mn} = \sqrt{D\left(\lambda_m^2 + \mu_n^2\right)^2 / \rho h}$ and $\tilde{P} = 16 P_0 / \pi^2 \rho h$. Applying the Runge-Kutta method Gives the deflection-time response which is shown below in Fig. 5 as a validation comparing Akay [1] with the present simplified isotropic case. The properties utilized for this validation are given as,

$$L_1 = L_2 = 0.25\,m,\ h = 0.05\,m$$

$$E = 206.1 GPa,\ \rho = 7848\ kg/m^3,\ \nu = 0.25$$

$$P_0 = 0.981\,MPa$$

By observation, it can be seen that very good agreement exists between Akay[1], who applied a finite element technique, and the present result, based on the Runge-Kutta technique. Any differences are due to the approximations made within the two different numerical approaches.

8.2 Validation of the Natural frequency

To further substantiate the validation, comparisons are made with Ramu and Mohanty [4] where the first ten natural frequency modes for a thin rectangular plate based on the linear CPT with simply supported plates for various plate thicknesses are presented. These comparisons are listed below in table 2. The geometrical and material properties associated with this data is given as

$$L_1 = 0.6m\ ,\ L_2 = 0.4m$$

$$E = 70\,GPa\ ,\ \rho = 2700\ kg/m^3,\ \nu = 0.3$$

Very good agreement is apparent for all ten modes for the first two plate thicknesses (0.00625m and 0.0125m). As the plate thickness becomes larger, while at the higher frequency modes, the marginal difference becomes larger. This is explained by the fact that the present theory for thin plates is less accurate for thicker plates. Although the differences remain small, the accurate prediction of the natural frequencies requires some of the elements of the thicker plate theory such as the inclusion of the transverse shear strain, normal strain, and the rotational strains.

8.3 Results for the Present Theory

The present theoretical results are provided for a variety of different types of pressure pulses which include a sonic-boom, a triangular pulse, a rectangular pulse, a step pulse, a sine pulse, and a traveling tangential shock wave. The effect of these pulse forms on the deflection-time response and the effect of varying the volume fraction indexes is presented and analyzed to evaluate how all of these effects interplay on the structural response. The material and geometrical properties adopted for the theoretical results are

$$L_1 = L_2 = 0.25\,m,\ h = 0.009525\ \ m$$

Ti-6Al-4V: $E = 105.7 \times 10^9\ Pa,\quad \nu = 0.298,\quad \rho = 4429\ kg/m^3$

Aluminum Oxide: $E = 320.2 \times 10^9\ Pa,\quad \nu = 0.260,\quad \rho = 3750\ kg/m^3.$

In Fig. 6, The deflection-time response due to a sonic boom is presented for three gradient measures according to the volume fraction indexes. The case for metal can be seen to produce the highest deflections with the lowest frequency of oscillation. As the gradient distribution becomes more refined, the peak deflection values are lower than its isotropic metal counterpart coupled with higher oscillation frequencies.

A traveling shock wave parallel to the plate and its effect on the deflection-time response is provided in Fig. 7. There exist very high central deformations for metal coupled with lower frequencies in contrast to ceramic with low deformation and higher frequencies. Between the two extremes lies the structural performance for the multidirectional case. Clearly if the desired effect is to leverage the benefits of a both material properties of the constituent materials, then multidirectional materials offer a great advantage over isotropic materials while offering the strength close to ceramic. Another observation in Fig. 7 reveals that the intensity of the shockwave decays much quicker for both ceramic as well as for the multidirectional case.

In Fig. 8, the effect of a degenerated sonic boom into a triangular pulse in contrast to the symmetric sonic boom appears to be less violent and decays much faster. Also it should be noted that a comparison between multidirectional grading and a symmetric unidirectional grading can be made. The case $[M = 1, N_1 = N_2 = 0.05]$ is very close to a symmetric unidirectional functional grading which occurs when the volume fraction indexes take on the values

$[M = 1, N_1 = N_2 = 0]$. This obviously reveals that a symmetric unidirectional functional grading performs better from a dynamic response standpoint than its multidirectional counterpart.

In Figs. (9)-(11), the effect a step pulse, a sine pulse, and a rectangular pulse are depicted. The same kind of competing behavior is observed between metal, ceramic, and multidirectional functional-type grading. Fig. 12 provides a comparison between sonic boom loadings for various magnitudes of the shock pulse factor. When the shock pulse factor, *r*=1, a triangular pulse presents itself, when *r*=2, a typical sonic boom-type loading is present, and when *r*=3, a nonsymmetrical sonic boom type loading develops. Comparisons between the three types gives in increasing order of shock pulse factor magnitude the order of most hostile response. The least damaging is the triangular pulse with the most violent response coming from the unsymmetrical sonic boom.

Conclusions

The dynamic response of multidirectional simply supported plates has been addressed through the application of several pressure pulses. Several validations have been made for the isotropic case. The implications of the volume fraction index on the material grading have been presented. Also, various types of pressure pulses and their effects on the deflection-time response of a thin rectangular plate based on the linear strain theory have been provided graphically and discussed. A combination of semi-analytical and numerical procedures were adopted to arrive at the governing response such as the Galerkin method, The Gaussian-Quadrature method for numerical integration, and the Rung-Kutta method to solve the governing response equation for the dynamic response.

It was revealed that multidirectional functionally graded plates provide better performance than their isotropic counterpart but decreased performance when compared with symmetric unidirectional functionally graded plates. It is hoped that this instrumental base in which to build upon will be realized in the development of more advanced theories.

Acknowledgement

The author would like to express thanks to the U.S. Army-RDECOM-TARDEC for their support and funding under the independent Laboratory In-House Research Program (ILIR).

Disclaimer

Reference herein to any specific commercial company, product, process, or service by trade name, trademark, manufacturer, or otherwise, does not necessarily constitute or imply its endorsement, recommendation, or favoring by the United States Government or the Department of the Army (DoA). The opinions of the authors expressed herein do not necessarily state or reflect those of the United States Government or the DoA, and shall not be used for advertising or product endorsement purposes.

References

[1] H.U. Akay, Dynamic Large Deflection Analysis of Plates Using Mixed Finite Elements, Computers and Structures, 11 (1980) 1-11.

[2] V. Birman, L.W. Byrd, Modeling and Analysis of Functionally Graded Materials and Structures, Applied Mechanics Reviews, 60 (2007) 195-216.

[3] V. Birman, L. Byrd, R. Chona, M.A. Haney, Response of spatially tailored structures to thermal loading, J. Eng Math, 61 (2008) 201-217.

[4] I. Ramu, S.C. Mohanty, Study on Free Vibration Analysis of Rectangular Plate Structures Using Finite Element Method, Procedia Engineering, 38 (2012) 2758-2766.

[5] L. Librescu, A. Nosier, Response of Laminated Composite Flat Panels to Sonic Boom and Explosive Blast Loadings, AIAA Journal, 28 (1990) 345-352.

[6] J.N. Reddy, Theory and Analysis of Elastic Plates and Shells, Second Edition, CRC Press, (2006)

Figure Captions

Fig 1. A pictorial representation of a simply supported multidirectional functionally graded plate exposed to a spherical blast above the plate.

Fig 2. The volume fraction as a function of the distance along the plate in the *x*-direction for various magnitudes of the volume fraction indexes N_1,

Fig 3. The volume fraction as a function of the distance along the plate in the *y*-direction for various magnitudes of the volume fraction indexes N_2.

Fig 4. The volume fraction as a function of the through-the-thickness z-coordinate direction for various volume fraction indexes

Fig 5. Validation of the amplitude of center deflection as a function of time for an isotropic plate.

Fig 6. Amplitude of center deflection as a function of time due to a sonic boom for a multidirectional functionally graded plate with varying degrees of the volume fraction indexes ($t_a = 0, t_p = 0.005$, $r = 2$, $P_0 = 0.15\,MPa$, $\Delta_{11} = 0.05$)

Fig 7. Amplitude of center deflection as a function of time due to a traveling tangential shockwave for a multidirectional functionally graded plate with varying degrees of the volume fraction indexes ($\eta = 0.5, c = 100\ \ m/s, P_0 = 0.15\,MPa$, $\Delta_{11} = 0.05$)

Fig 8. Amplitude of center deflection as a function of time due to a triangular blast for a multidirectional functionally graded plate with varying degrees of the volume fraction indexes ($t_a = 0, t_p = 0.005$, $r = 1$, $P_0 = 0.15\,MPa$, $\Delta_{11} = 0.05$)

Fig 9. Amplitude of center deflection as a function of time due to a step pulse for a multidirectional functionally graded plate with varying degrees of the volume fraction indexes ($t_a = 0, t_p = \infty$, $r = 1$, $P_0 = 0.15\,MPa$, $\Delta_{11} = 0.05$)

Fig 10. Amplitude of center deflection as a function of time due to a sine pulse for a multidirectional functionally graded plate with varying degrees of the volume fraction indexes ($t_p = 0.005$, $P_0 = 0.15\,MPa$, $\Delta_{11} = 0.05$)

Fig 11. Amplitude of center deflection as a function of time due to a rectangular pulse for a multidirectional functionally graded plate with varying degrees of the volume fraction indexes ($t_p = 0.005, P_0 = 0.15\,MPa, \Delta_{11} = 0.05$)

Fig. 12. Amplitude of center deflection as a function of time due to a sonic boom with varying degrees of the shock pulse factor *r* for a multidirectional functionally graded plate ($t_a = 0, t_p = 0.005, P_0 = 0.15\,MPa, \Delta_{11} = 0.05$)

Tables

Table 1. The effect of the volume fraction indexes on the grading-type.

Grading-Type	N_1	N_2	M	**Volume Fraction,** V_1
Isotropic Metal, P_2	0 ($N_1 > 3$)	0 ($N_2 > 3$)	$M > 20$	0
Isotropic Ceramic, P_1	0	0	0	1
Unidirectional Symmetric	0	0	1	$V_1 = V_1(z)$
Bi-Directional (x-y Plane)	$0 < N_1 < 3$	$0 < N_2 < 3$	0	$V_1 = V_1(x, y)$
Bi-Directional (x-z Plane)	$0 < N_1 < 3$	0	$0 < M < 20$	$V_1 = V_1(x, z)$
Bi-Directional (y-z Plane)	0	$0 < N_2 < 3$	$0 < M < 20$	$V_1 = V_1(y, z)$
Multi-Directional	$0 < N_1 < 3$	$0 < N_2 < 3$	$0 < M < 20$	$V_1 = V_1(x, y, z)$

Table 2. Comparison of the natural frequency ω (Hz) for a simply supported thin Isotropic plate.

	Plate Thickness 0.00625m		Plate Thickness 0.0125m		Plate Thickness 0.025m		Plate Thickness 0.05m	
Mode	Present	Exact[4]	Present	Exact[4]	Present	Exact[4]	Present	Exact[4]
m=1,n=1	136.4	136.5	272.8	273.1	545.7	546.2	1091.4	1092.5
m=2,n=1	262.4	262.6	524.7	525.2	1049.4	1050.4	2098.9	2100.9
m=1,n=2	419.8	420.1	839.5	840.3	1679.1	1680.7	3358.2	3361.5
m=3,n=1	472.2	472.7	944.5	945.4	1889.0	1890.8	3777.9	3781.7
m=2,n=2	545.7	546.2	1091.4	1092.5	2182.8	2185.0	4365.6	4370.1
m=3,n=2	755.6	756.35	1511.2	1512.7	3022.3	3025.4	6044.7	6050.8
m=4,n=1	766.1	766.85	1532.2	1533.7	3064.3	3067.4	6128.7	6134.8
m=1,n=3	892.0	892.9	1784.0	1785.8	3568.1	3571.6	7136.1	7143.3
m=2,n=3	1017.9	1018.9	2035.9	2037.9	4071.8	4075.9	8143.6	8151.82
m=4,n=2	1049.4	1050.4	2098.9	2100.9	4197.7	4201.9	8395.4	8403.9

Figures (In numerical Order)

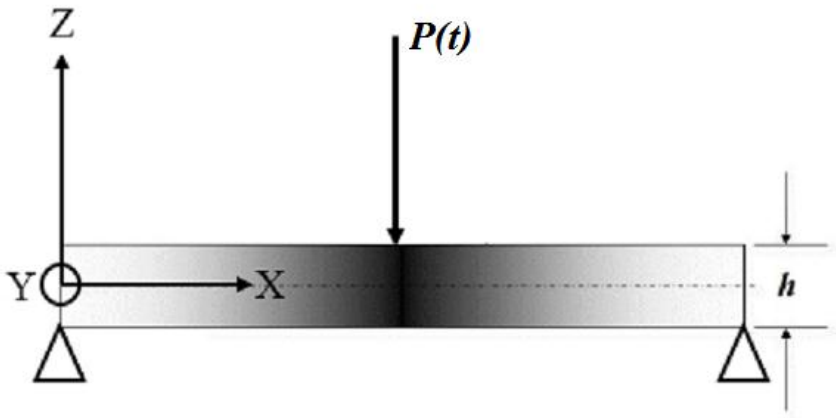

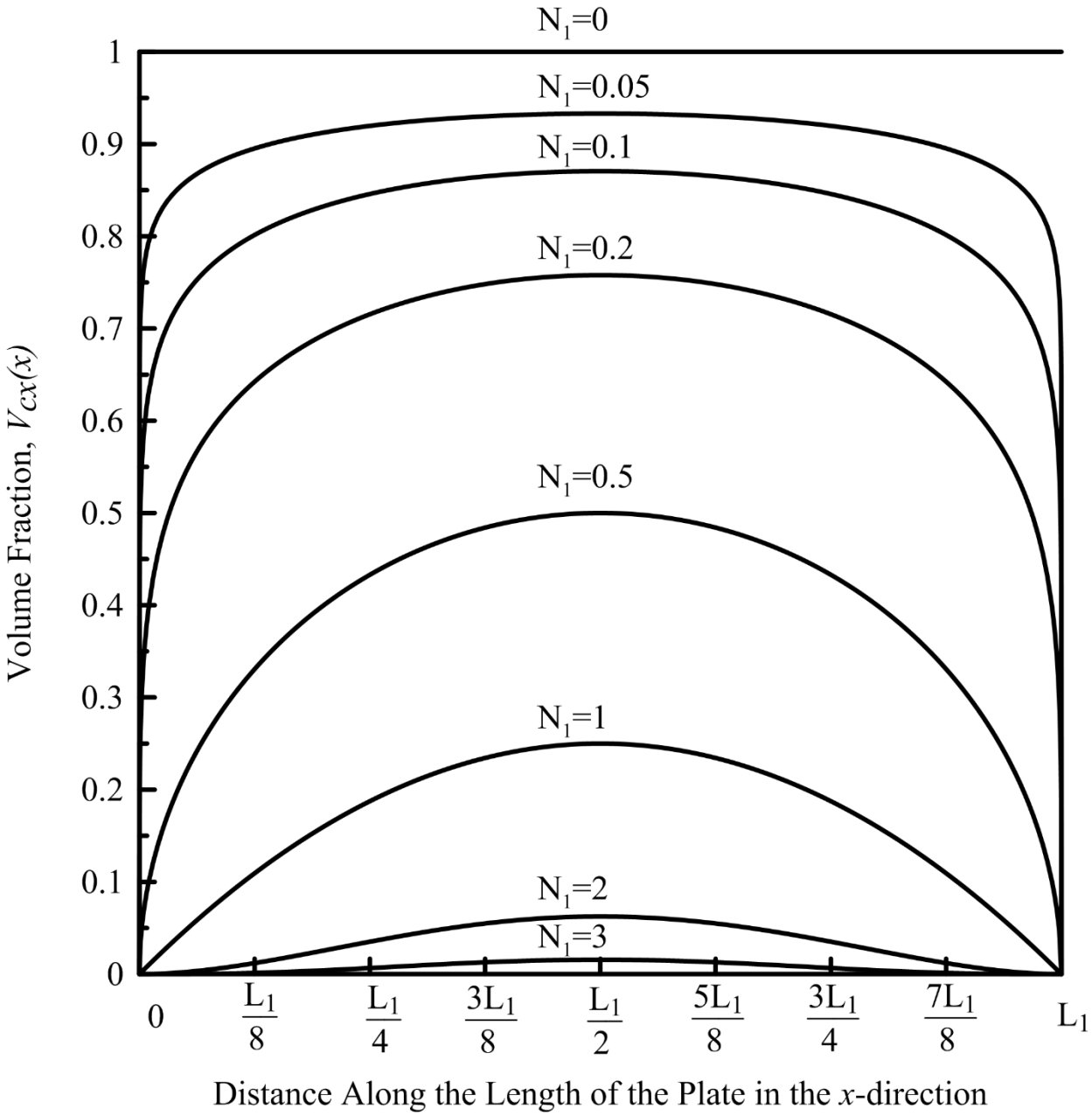
N1=0
N1=0.05
N1=0.1
N1=0.2
N1=0.5
N1=1
N1=2
N1=3
1
0.9
0.8
0.7
0.6
0.5
0.4
0.3
0.2
0.1
0
Volume Fraction, Vcx(x)
0
L1/8
L1/4
3L1/8
L1/2
5L1/8
3L1/4
7L1/8
L1
Distance Along the Length of the Plate in the x-direction

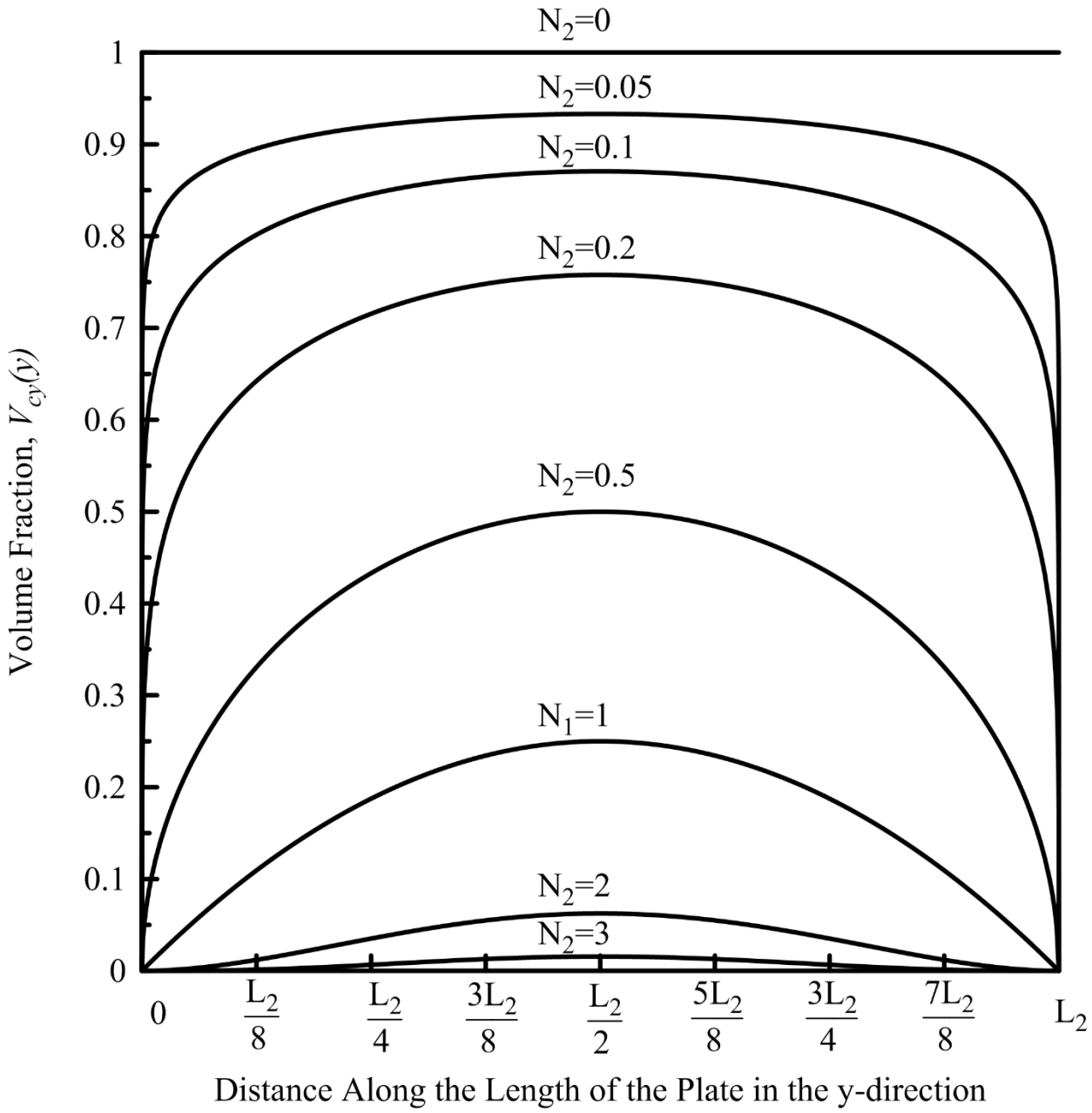
N2=0
N2=0.05
N2=0.1
N2=0.2
N2=0.5
N1=1
N2=2
N2=3
Volume Fraction, Vcy(y)
1
0.9
0.8
0.7
0.6
0.5
0.4
0.3
0.2
0.1
0
0
L2/8
L2/4
3L2/8
L2/2
5L2/8
3L2/4
7L2/8
L2
Distance Along the Length of the Plate in the y-direction

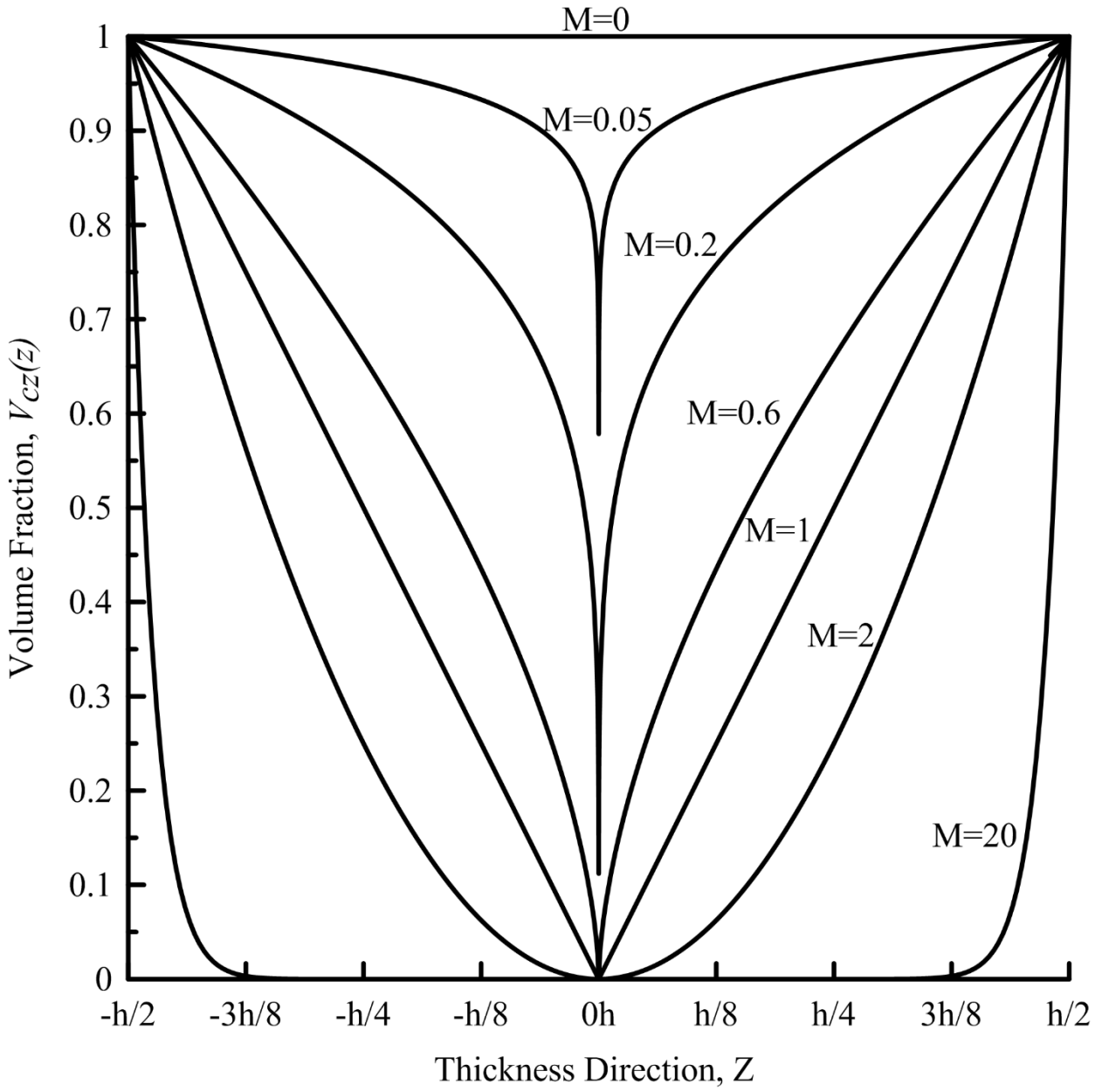
M=0
M=0.05
M=0.2
M=0.6
M=1
M=2
M=20
1
0.9
0.8
0.7
0.6
0.5
0.4
0.3
0.2
0.1
0
Volume Fraction, $V_{cz}(z)$
-h/2
-3h/8
-h/4
-h/8
0h
h/8
h/4
3h/8
h/2
Thickness Direction, Z

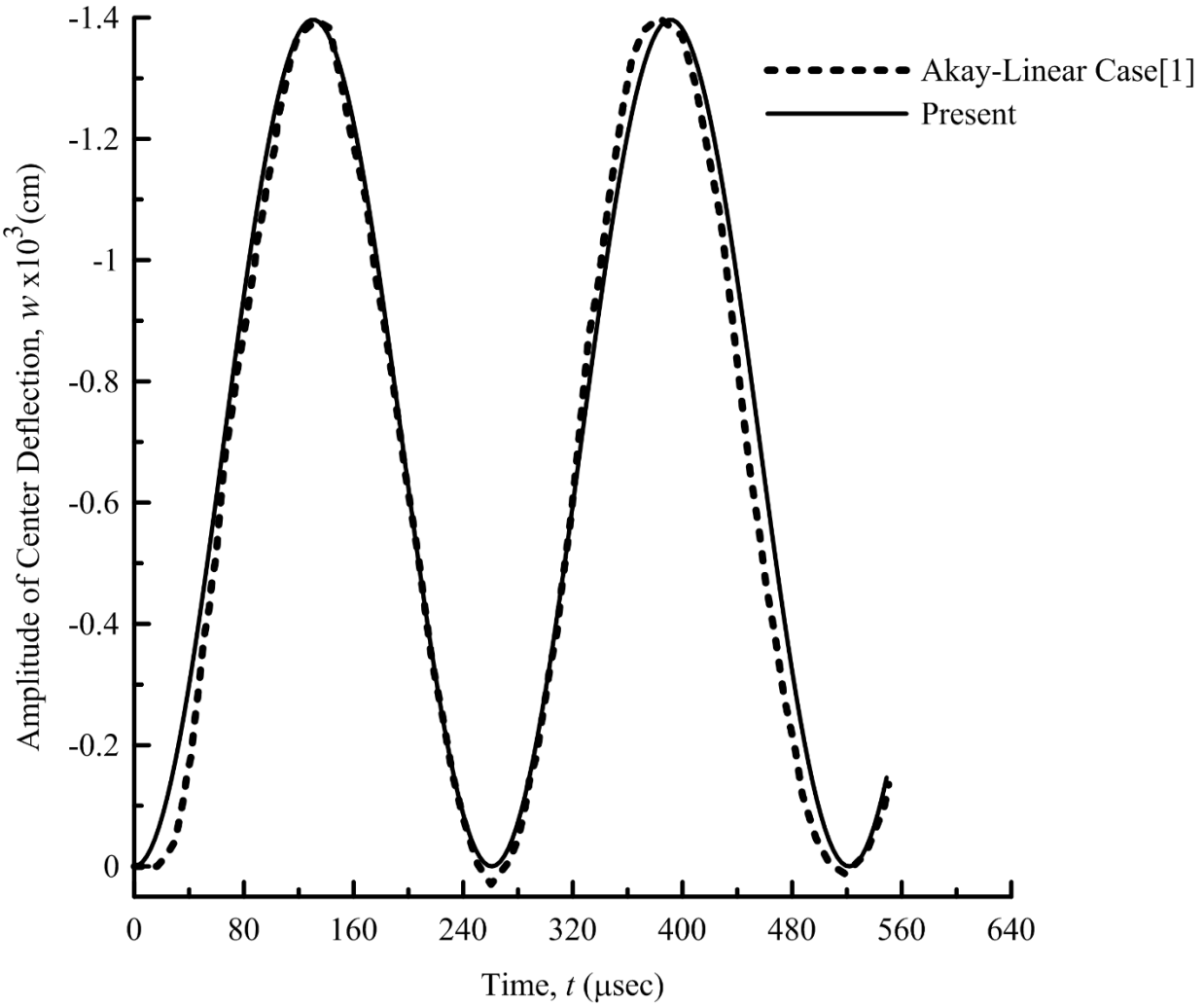
Akay-Linear Case[1]
Present
Amplitude of Center Deflection, w x10^3(cm)
-1.4
-1.2
-1
-0.8
-0.6
-0.4
-0.2
0
0
80
160
240
320
400
480
560
640
Time, t (μsec)

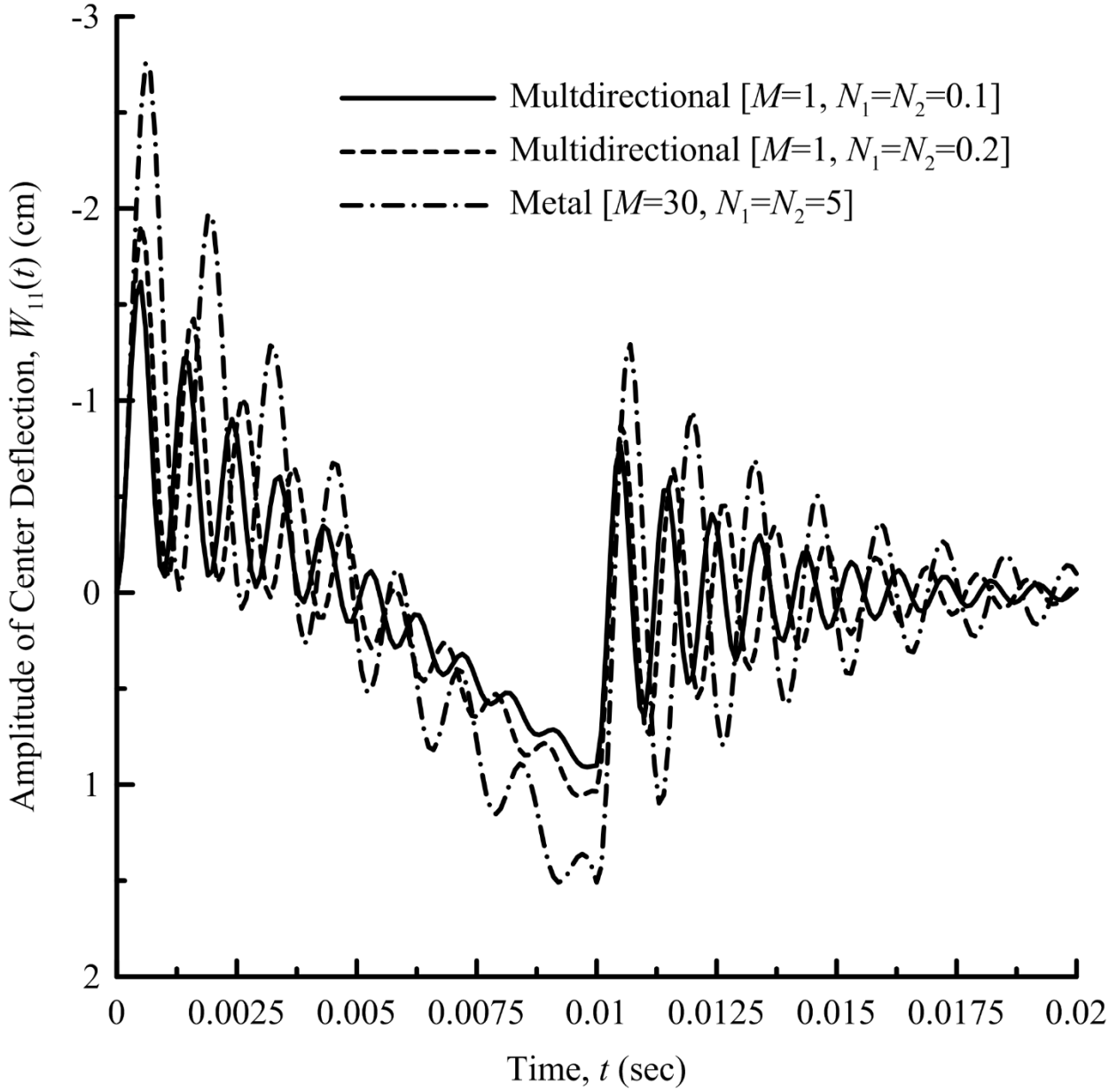
Multdirectional [M=1, N1=N2=0.1]
Multidirectional [M=1, N1=N2=0.2]
Metal [M=30, N1=N2=5]
Amplitude of Center Deflection, W11(t) (cm)
-3
-2
-1
0
1
2
0
0.0025
0.005
0.0075
0.01
0.0125
0.015
0.0175
0.02
Time, t (sec)

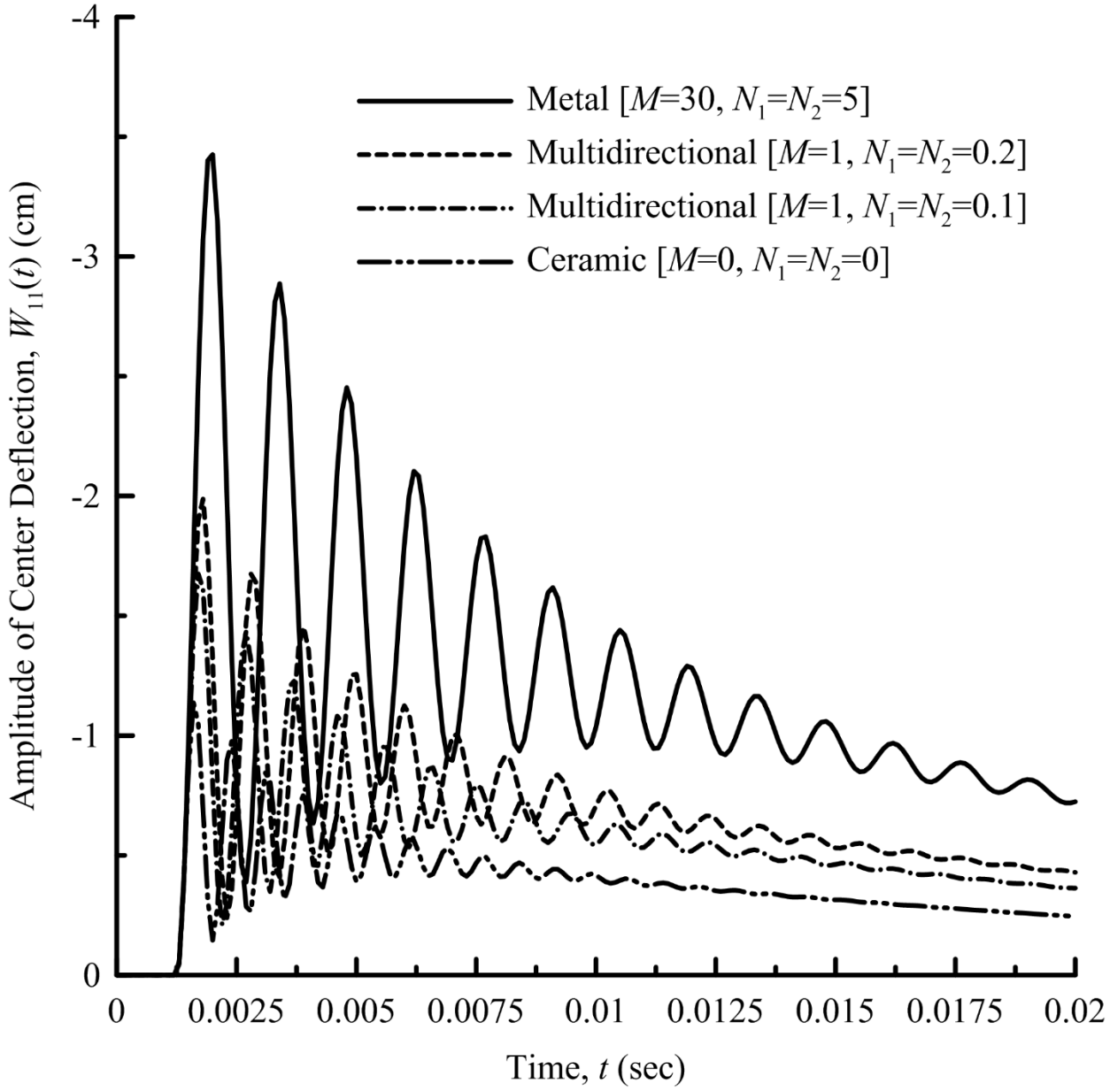
Metal [M=30, N1=N2=5]
Multidirectional [M=1, N1=N2=0.2]
Multidirectional [M=1, N1=N2=0.1]
Ceramic [M=0, N1=N2=0]
Amplitude of Center Deflection, W11(t) (cm)
-4
-3
-2
-1
0
0
0.0025
0.005
0.0075
0.01
0.0125
0.015
0.0175
0.02
Time, t (sec)

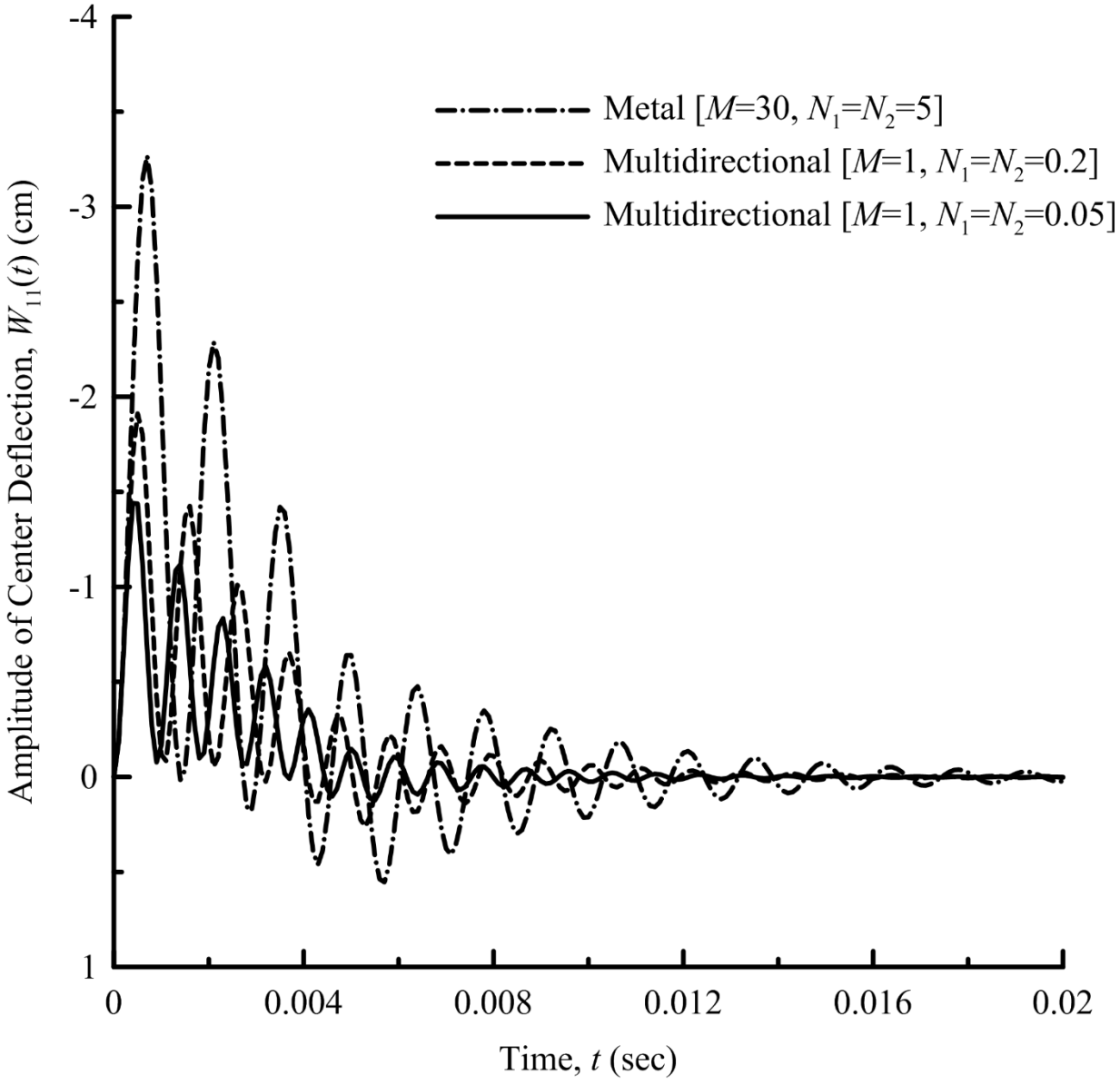
Metal [M=30, N1=N2=5]
Multidirectional [M=1, N1=N2=0.2]
Multidirectional [M=1, N1=N2=0.05]
Amplitude of Center Deflection, W11(t) (cm)
-4
-3
-2
-1
0
1
0
0.004
0.008
0.012
0.016
0.02
Time, t (sec)

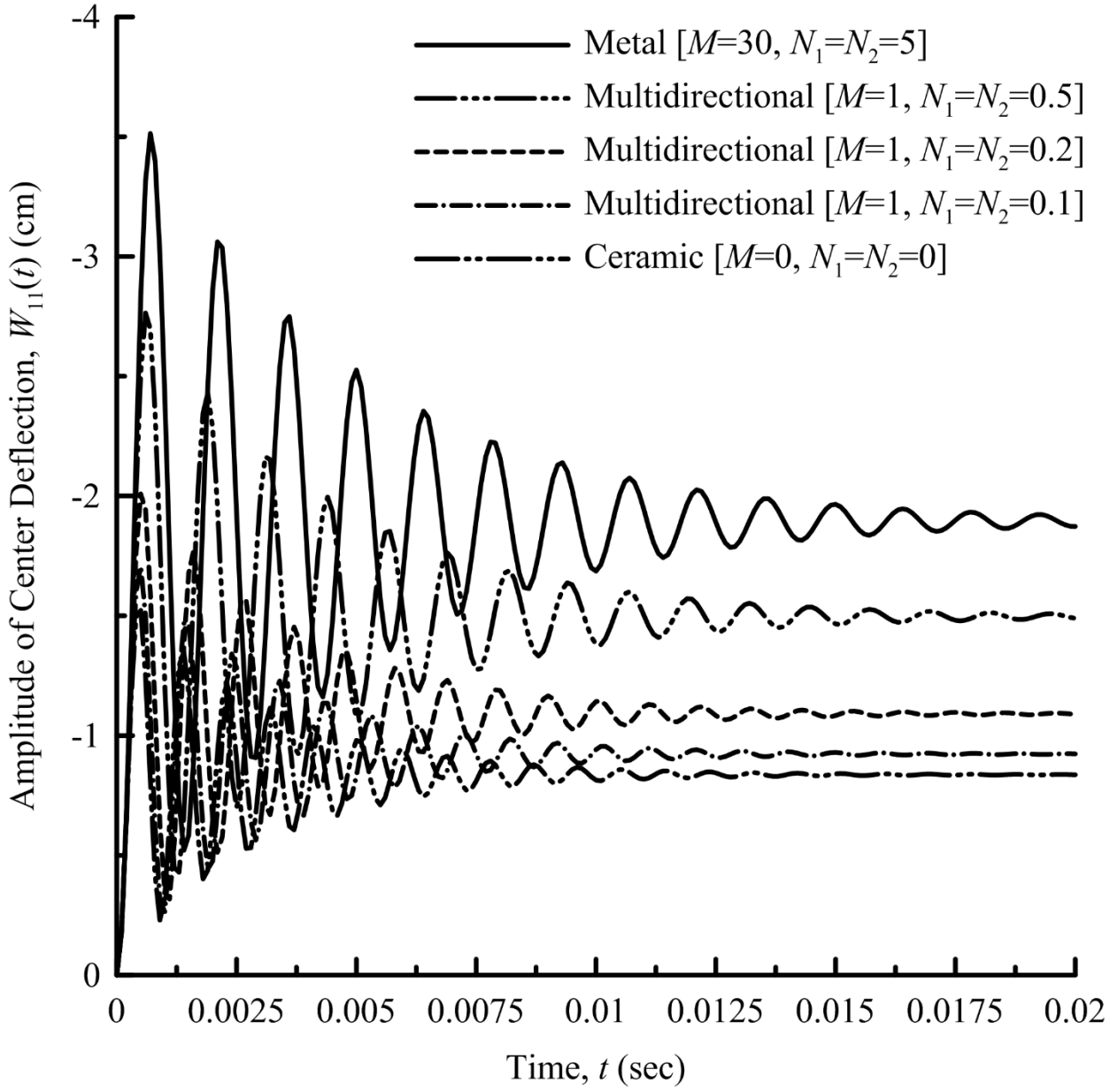
Metal [M=30, N1=N2=5]
Multidirectional [M=1, N1=N2=0.5]
Multidirectional [M=1, N1=N2=0.2]
Multidirectional [M=1, N1=N2=0.1]
Ceramic [M=0, N1=N2=0]
Amplitude of Center Deflection, W11(t) (cm)
-4
-3
-2
-1
0
0
0.0025
0.005
0.0075
0.01
0.0125
0.015
0.0175
0.02
Time, t (sec)

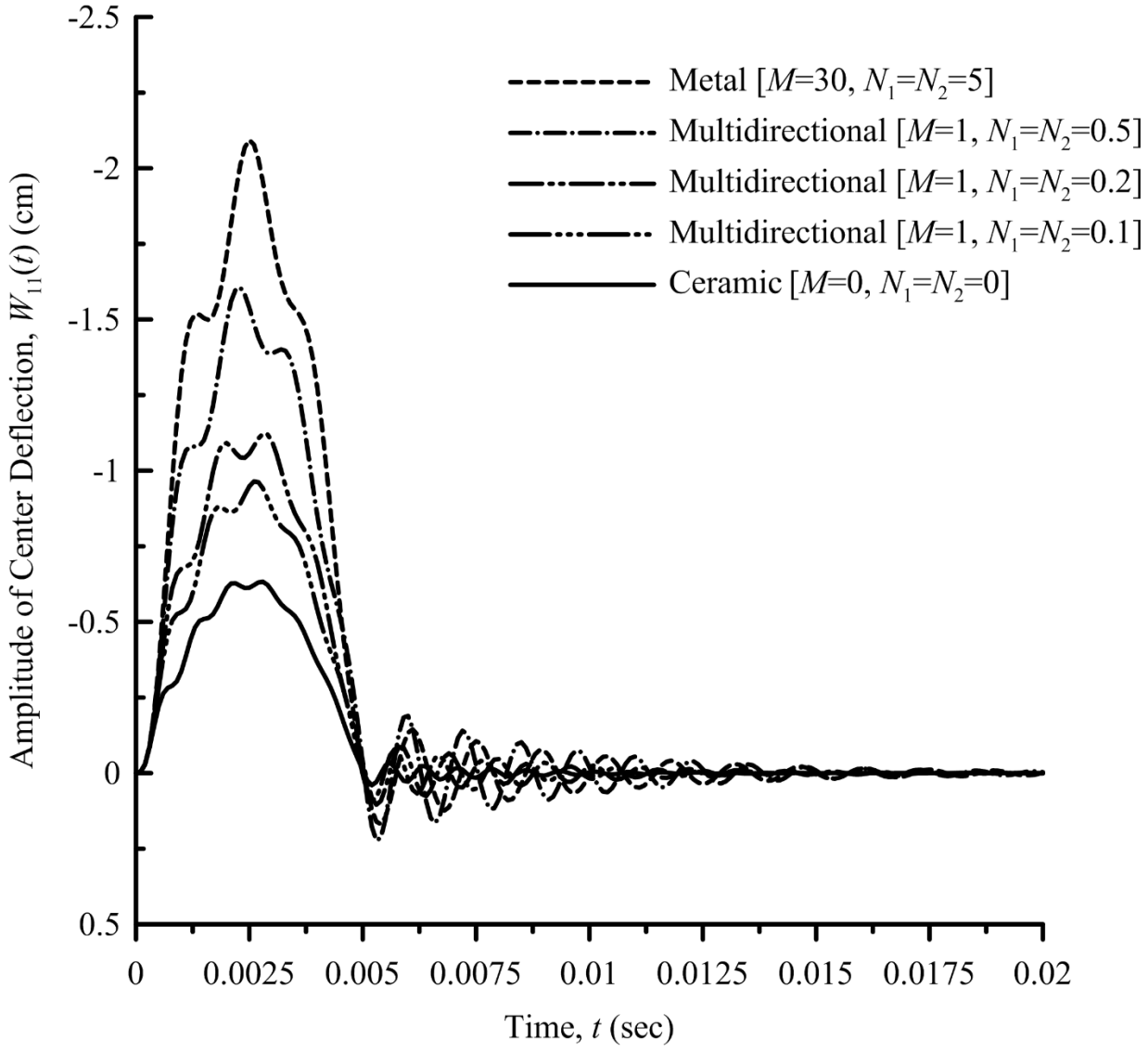
Metal [M=30, N1=N2=5]
Multidirectional [M=1, N1=N2=0.5]
Multidirectional [M=1, N1=N2=0.2]
Multidirectional [M=1, N1=N2=0.1]
Ceramic [M=0, N1=N2=0]
Amplitude of Center Deflection, W11(t) (cm)
-2.5
-2
-1.5
-1
-0.5
0
0.5
0
0.0025
0.005
0.0075
0.01
0.0125
0.015
0.0175
0.02
Time, t (sec)

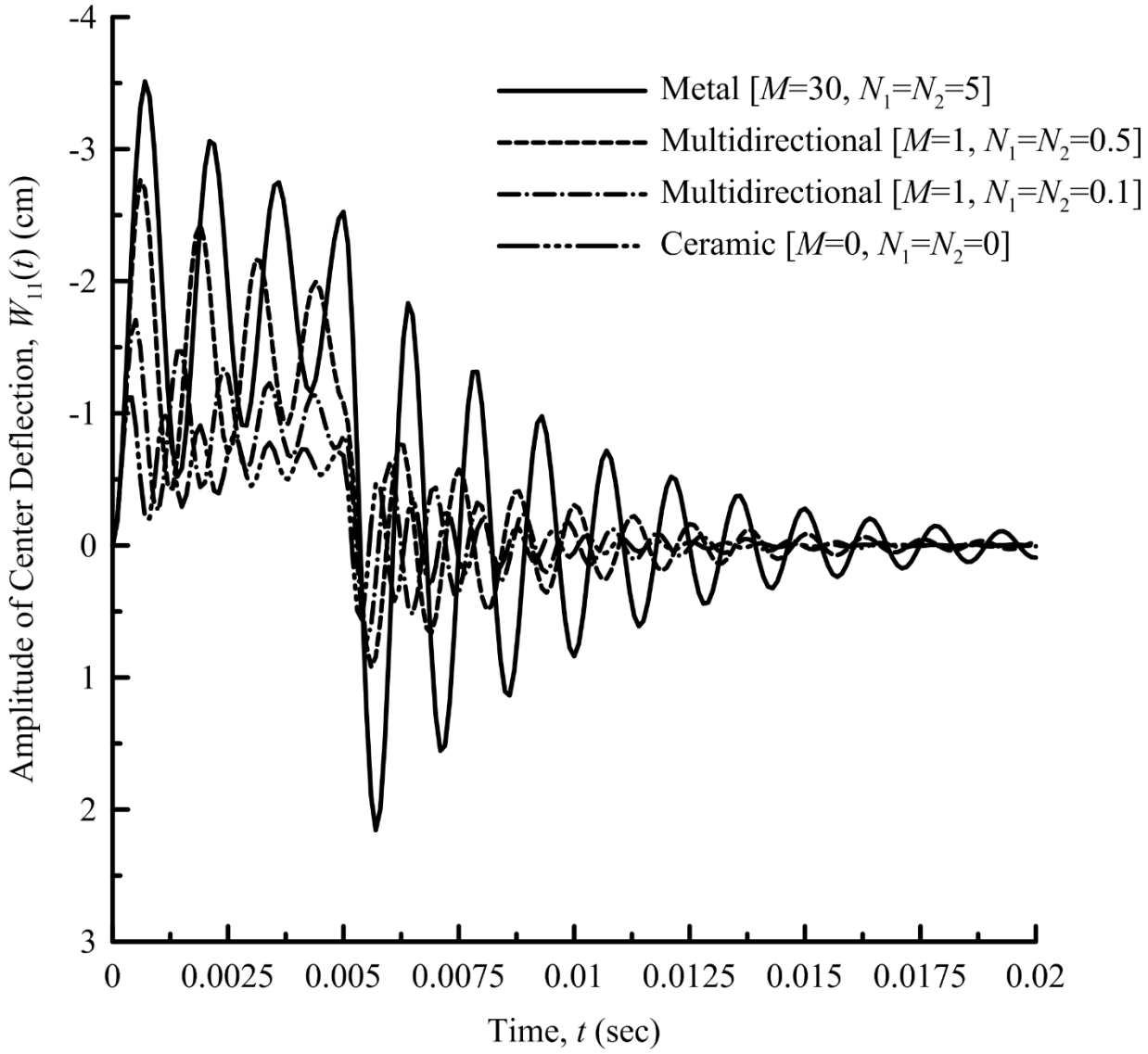
Metal [M=30, N1=N2=5]
Multidirectional [M=1, N1=N2=0.5]
Multidirectional [M=1, N1=N2=0.1]
Ceramic [M=0, N1=N2=0]
Amplitude of Center Deflection, W11(t) (cm)
Time, t (sec)
-4
-3
-2
-1
0
1
2
3
0
0.0025
0.005
0.0075
0.01
0.0125
0.015
0.0175
0.02

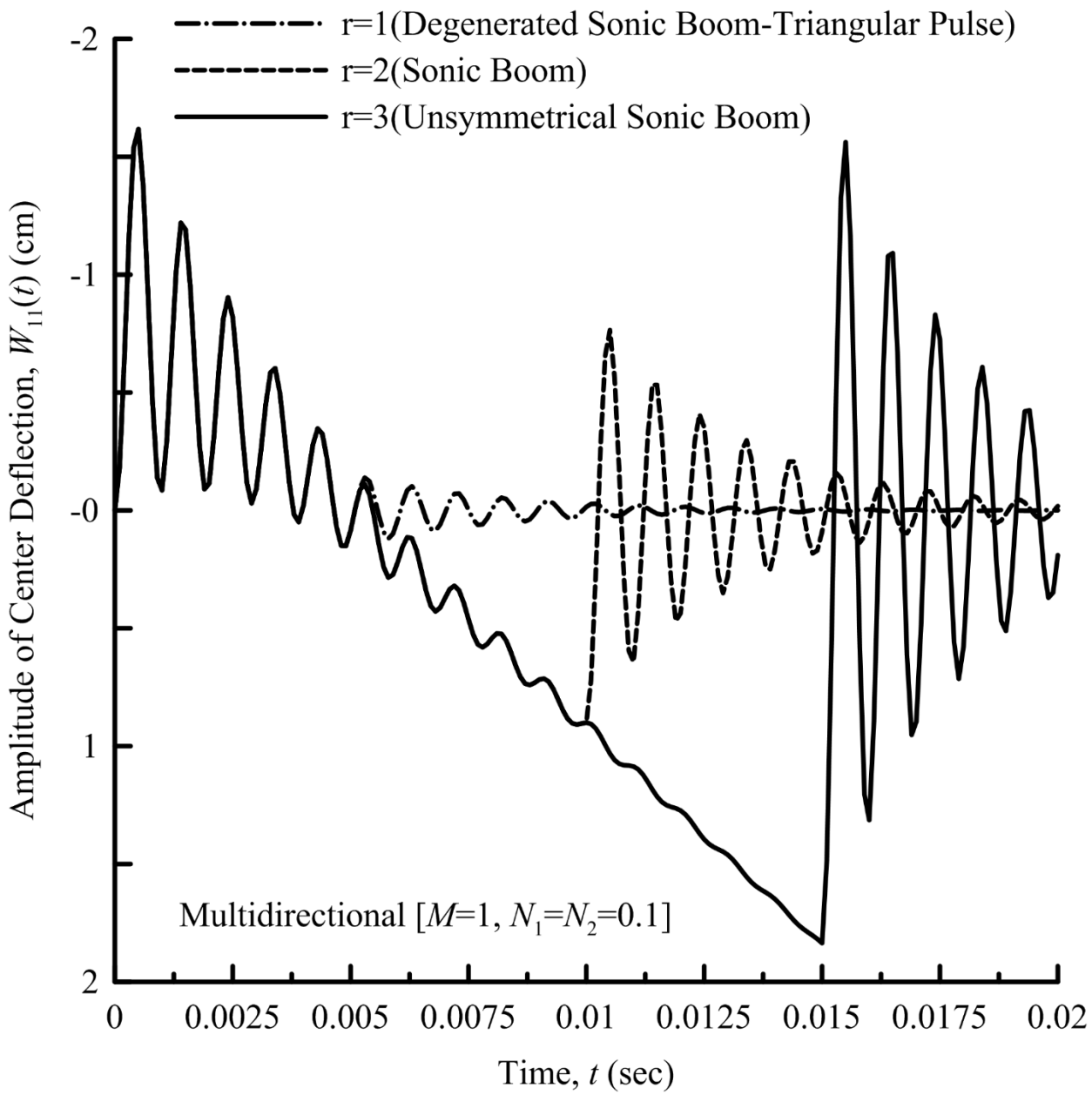
r=1(Degenerated Sonic Boom-Triangular Pulse)
r=2(Sonic Boom)
r=3(Unsymmetrical Sonic Boom)
Amplitude of Center Deflection, $W_{11}(t)$ (cm)
-2
-1
-0
1
2
Multidirectional [M=1, N_1=N_2=0.1]
0
0.0025
0.005
0.0075
0.01
0.0125
0.015
0.0175
0.02
Time, t (sec)